Research Square

Preprints are preliminary reports that have not undergone peer review.
They should not be considered conclusive, used to inform clinical practice,
or referenced by the media as validated information.

Turning instability into functionality: Stoichiometry- and moisture-tuned reversible multichromism in Ethylammonium perovskites

Soohyung Park

soohyung.park@kist.re.kr

Korea Institute of Science and Technology https://orcid.org/0000-0002-6589-7045

Aelim Ha

Korea Institute of Science and Technology

Seunghwan Kim

Korea Institute of Science and Technology

Kitae Kim

Yonsei University

Eunki Yoon

Korea Institute of Science and Technology

Sooyeon Pak

Korea Institute of Science and Technology

Yeonjin Yi

Yonsei University https://orcid.org/0000-0003-4944-8319

Dongguen Shin

Chonnam National University https://orcid.org/0000-0002-3601-942X

Young Yong Kim

Pohang University of Science & Technology https://orcid.org/0000-0001-6102-9518

Kyu Hyoung Lee

Yonsei University https://orcid.org/0000-0001-6843-6706

Article

Keywords:

Posted Date: April 15th, 2026

DOI: https://doi.org/10.21203/rs.3.rs-9305944/v1

License: This work is licensed under a Creative Commons Attribution 4.0 International License.
Read Full License

Additional Declarations: There is **NO** Competing Interest.

Turning instability into functionality: Stoichiometry- and moisture-tuned reversible multichromism in Ethylammonium perovskites

Aelim Ha[1,2], Seunghwan Kim[1,3], Kitae Kim[1,3], Eunki Yoon[1,2], Sooyeon Pak[1,3], Yeonjin Yi[3], Dongguen Shin[4], Young Yong Kim[5,*], KyuHyoung Lee[2,*], and Soohyung Park[1,6,*]

[1]Advanced Analysis Center, Korea Institute of Science and Technology (KIST), Seoul 02792, Republic of Korea

[2]Department of Materials Science & Engineering, Yonsei University, 50 Yonsei-ro, Seodaemun-gu, Seoul 03722, Republic of Korea

[3]Department of Physics, Yonsei University, 50 Yonsei-ro, Seodaemun-gu, Seoul 03722, Republic of Korea

[4]Department of Physics, Chonnam National University, 77 Yongbong-ro, Buk-gu, Gwangju 61186, Republic of Korea

[5]Beamline Division, Pohang Accelerator Laboratory, Pohang University of Science and Technology, Pohang, 37673, Republic of Korea

[6]Division of Nano & Information Technology, KIST School, University of Science and Technology (UST), Seoul 02792, Republic of Korea

*Corresponing author e-mail

kimyy@postech.ac.kr, khlee2018@yonsei.ac.kr, soohyung.park@kist.re.kr

Abstract

Organic–inorganic hybrid perovskites located at the boundaries of the Goldschmidt tolerance factor exhibit a structural softness that affords unique stimuli responsiveness but complicates their intrinsic phase stability. Ethylammonium (EA)-based perovskites, in particular, have long suffered from ambiguous and conflicting crystallographic reports, with their responses to moisture environments often misinterpreted as irreversible chemical degradation. Here, we resolve this long-standing structural ambiguity by identifying environmental humidity as a hidden variable whose impact is critically gated by precursor stoichiometry. We demonstrate that reaching a specific compositional threshold ([EAI]/[PbI_2] ≥ 1.6) transforms the otherwise structurally rigid or degradation-prone perovskite lattice into a highly flexible mixed-dimensional landscape. Within this responsive regime, moisture triggers a rapid, synchronized, and fully reversible reconfiguration between 1D- and 2D-related structural motifs, that we call a dynamic lattice rearrangement, without chemical decomposition (PbI_2 formation), which manifests as a repeatable multicolor hydrochromism. Practically leveraging this stoichiometry-gated dynamics, we successfully demonstrate zero-power, autonomous smart windows that adapt to external weather conditions, as well as dual-functional medical moisture indicators capable of both irreversible moisture history logging and real-time quantitative monitoring. This work establishes a new paradigm for boundary-region perovskites, turning their inherent instability into innovative functionality for active environmental sensing and smart optoelectronic devices.

1. Introduction

Organic–inorganic hybrid perovskites have emerged as a premier class of optoelectronic materials, driven by their outstanding optoelectronic efficiencies and high structural tunability [1-10]. The stability of these crystal structures and their susceptibility to distortion are generally rationalized by the Goldschmidt tolerance factor[11-13]. Materials residing near the boundaries of this stability window are of particular interest, as they occupy a regime of structural softness characterized by the coexistence of competing phases and local lattice distortions[14,15]. While this inherent flexibility renders them highly sensitive to external stimuli, such as temperature[16-18], pressure[19-21], and light[22,23], it simultaneously poses significant challenges in stabilizing bulk phases and precisely defining their intrinsic material properties.[24,25]

Among these boundary-region systems, Ethylammonium (EA)-based perovskites represent a prominent yet poorly understood example. Despite predictions placing the EA cation outside the conventional stability window for 3D perovskites[12,26], reports on its structural behavior have remained highly inconsistent[27-30]. For instance, contemporaneous and directly contradictory observations continue to emerge in the literature; Muralidhar *et al.* reported a 1D structure[27], whereas Guvenc *et al.* identified a 2D with 3D configuration[28]. This pronounced structural ambiguity implies that the phase behavior of EA-based perovskites is governed by underlying factors that are neither fully controlled nor understood. Consequently, EA-based perovskites have largely been marginalized in systematic structure–property correlation studies, and their responses to environmental stimuli have often been dismissed as obscure or secondary (extrinsic) artifacts.

Here, we hypothesize that these conflicting reports stem from an uncontrolled experimental parameter, environmental humidity[31-34] acting as a hidden variable, and that its impact is critically gated by precursor stoichiometry, a factor largely overlooked in previous studies. Unlike Methylammonium (MA)-based perovskites, where moisture typically drives irreversible degradation into PbI_2[35], systems incorporating larger cations (such as EA) can support the reversible structural accommodation of water molecules, provided the lattice exhibits sufficient flexibility. However, it is highly probable that such humidity-driven lattice dynamics have been either misinterpreted as chemical degradation or entirely overlooked due to the arbitrary variations in precursor ratios employed across different investigations.

To resolve this ambiguity, we present a systematic investigation into the coupled effects of

precursor stoichiometry and environmental humidity on the structural evolution of EA-based perovskites. Utilizing *in-situ* grazing-incidence wide-angle X-ray scattering (GIWAXS) and optical spectroscopy, we map the dynamic phase landscape of these materials. We identify a distinct stoichiometric threshold ([EAI]/[PbI_2] ≈ 1.6). Below this threshold, the lattice remains rigid or degrades irreversibly. Conversely, above it, the material enters a responsive regime where moisture triggers a rapid, non-destructive, and fully reversible structural reconfiguration between 1D- and 2D-related motifs.

This work transforms the perceived instability of EA-based perovskites into a highly functional feature. We demonstrate that this reversible lattice dynamics gives rise to a repeatable multicolor hydrochromism, distinctly decoupled from chemical decomposition. This establishes EA-based perovskites as a premier model system for directly exploring reversible lattice dynamics at the extreme boundaries of the Goldschmidt tolerance factor. Furthermore, by leveraging this stoichiometry-gated responsiveness to demonstrate humidity-controlled smart devices, including moisture-responsive chromic windows and humidity indicators, we provide a new paradigm for utilizing structurally flexible perovskites in active environmental applications.

2. Results

2.1. Composition-dependent structural dimensionality

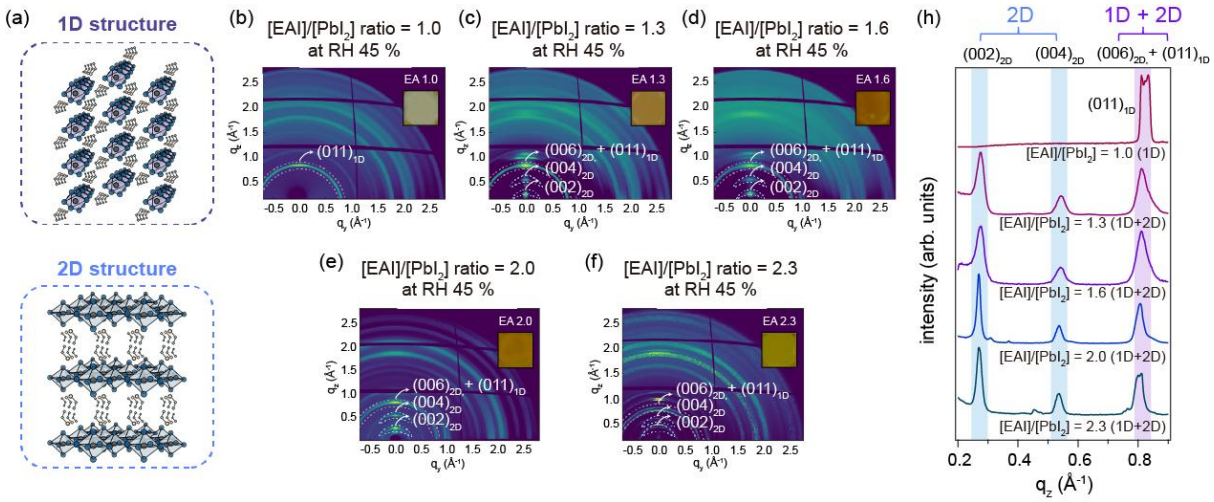


Figure 1 GIWAXS analysis of composition-dependent structural dimensionality in EA-based perovskite thin films. (a) Schematic illustrations of representative perovskite connectivities: (top) a 1D-related structure composed of isolated chains of face-sharing PbI_6 octahedra, and (bottom) a layered 2D-related structure consisting of extended inorganic PbI_6 octahedral sheets separated by Ethylammonium (EA^+) spacer cations. (b-f) *Ex-situ* GIWAXS patterns of EA-based perovskite thin films prepared with systematically varied [EAI]/[PbI_2] ratios, revealing composition-dependent structural dimensionality. (h) The 1D out-of-plane GIWAXS diffraction profiles highlight a structural evolution from a purely 1D phase (violet) to a mixed-dimensional structure comprising both 2D-layered and 1D phases as the [EAI]/[PbI_2] ratio increases.

To establish the structural foundation for the humidity-driven phase dynamics discussed later, we first mapped the initial, static crystallographic landscape of the EA-based perovskite thin films as a function of precursor stoichiometry at a fixed relative humidity of 45%. The precursor stoichiometry was verified through XPS measurements (Figure S1 and Table S1). We found that, rather than forming a single uniform phase, tuning the [EAI]/[PbI_2] ratio continuously modulates the balance between competing one-dimensional (1D) and two-dimensional (2D) structural motifs, thereby creating a mixed-dimensional structural landscape.

Ex-situ grazing-incidence wide-angle X-ray scattering (GIWAXS) measurements reveal this composition-driven structural evolution (Figure 1b-f). Films prepared with an [EAI]/[PbI_2] ratio of 1.0 exhibit a diffuse Debye–Scherrer ring centered at $q \approx 0.81$ Å^{-1}. This feature is characteristic of a predominantly 1D-related perovskite framework (Figure S2 and Table S2)

composed of randomly oriented, isolated chains of PbI_6 octahedra (Figure 1a, top) [27]. As the ratio increases to 1.3 and above, this 1D-related diffraction feature persists but develops azimuthal anisotropy with enhanced intensity near $\chi \approx 90°$, indicating the emergence of an out-of-plane preferred orientation.

Concurrently, increasing the EA content introduces additional diffraction peaks at 0.26, 0.54 $Å^{-1}$ (Figure 1c-f and Table S3). These reflections correspond to the long-range periodicity of layered 2D-related motifs, which are characterized by extended inorganic octahedral sheets separated by EA spacer cations (Figure 1a, bottom). The out-of-plane GIWAXS profiles further elucidate that the relative intensity of these 2D-related reflections systematically increases with higher [EAI]/[PbI_2] ratios. This progressive evolution signifies a gradual incorporation of layered ordering rather than an abrupt phase transformation. (Figure 1h)

Collectively, these static structural characteristics demonstrate that EA-based perovskites reside in a highly flexible regime where precursor stoichiometry dictates the coexistence of 1D and 2D connectivities. This baseline mixed-dimensional landscape is of paramount importance, as it provides the inherent structural softness required to accommodate the moisture-triggered dynamic lattice responses investigated in the following section.

2.2. Reversible humidity-driven phase and optical transitions

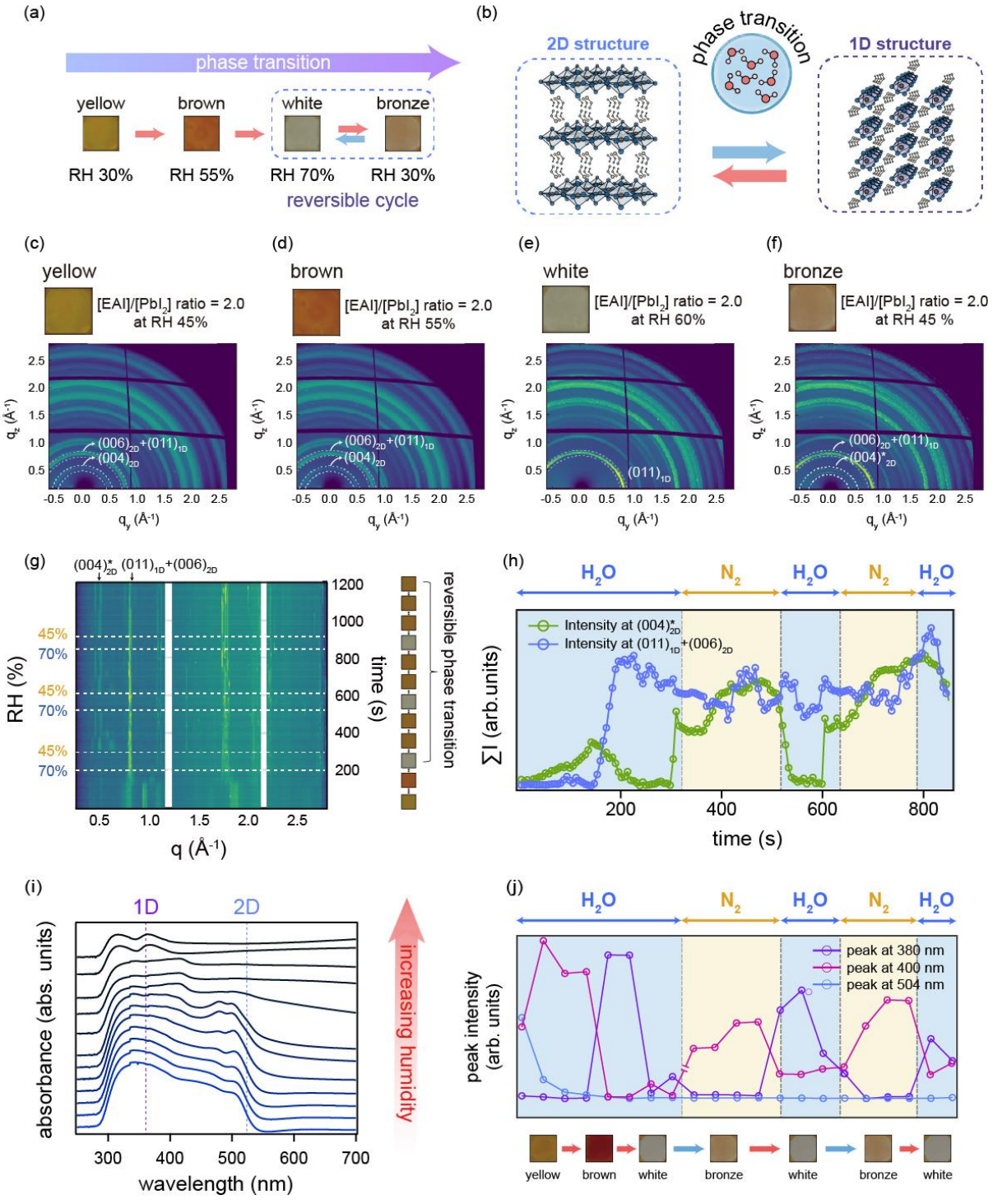


Figure 2 | Synchronization of humidity-driven phase and optical transitions in EA-based perovskites. (a) Optical photographs of the representative [EAI]/[PbI_2] ratio of 2.0 film, demonstrating the fully reversible multicolor hydrochromism (spanning yellow, brown, white, and bronze states) under cyclic relative humidity (RH) modulation. (b) Schematic

representation of the reversible structural rearrangement between the 2D layered and the 1D chain structure induced by moisture. (**c-f)** Representative GIWAXS patterns acquired at distinct optical states (yellow, brown, white, and bronze), confirming the corresponding structural configurations associated with each color state. The notation (004)* denotes a minor structural variant that shares the same basic framework as the 2D layered (004) motif but undergoes modifications induced by external structural stimuli. Note that the (002) diffraction peak is not visible in these *in-situ* GIWAXS plots because the beam stopper position was specifically adjusted to optimize real-time monitoring efficiency. **(g)** *In-situ* GIWAXS intensity heatmap recorded during repeated humidity cycling, highlighting reversible structural changes as a function of time. **(h)** Integrated intensities of characteristic 2D- ($(004)^*_{2D}$) and 1D-related ($(006)_{2D}$ + $(011)_{1D}$) diffraction peaks extracted from the *in-situ* GIWAXS data, showing synchronized and repeatable intensity variations over multiple humidity cycles. The corresponding integrated intensity plots for other precursor stoichiometries are provided in Figure S8 **(i)** UV–visible absorption spectra of [EAI]/[PbI_2] ratio of 2.0 measured under varying controlled humidity (1st cycle, RH from 45% to 70%) **(j)** Extracted absorbance at characteristic wavelengths associated with 1D-related (≈380 nm) and 2D-related (≈504 nm) optical transitions during repeated humidity cycling (detailed spectra provided in Figure S9).

While *ex-situ* measurements successfully revealed the composition-dependent mixed-dimensional landscape, such static analyses alone cannot fully elucidate the temporal sequence, reversibility, and underlying structural mechanisms of the phase transitions. Because the observed macroscopic optical changes occur rapidly on the timescale of tens of seconds, real-time monitoring is imperative to capture these dynamic lattice responses. To address this, we integrated *in-situ* grazing-incidence wide-angle X-ray scattering (GIWAXS) and ultraviolet-visible (UV-vis) spectroscopy to simultaneously track the structural and optical evolution of EA-based perovskites under cyclically controlled humidity.

Under cyclic humidity variations (RH 45% ↔ 70%), films with [EAI]/[PbI_2] ratio of 2.0 content exhibit pronounced and repeatable multicolor chromism. Notably, the [EAI]/[PbI_2] ratio of 2.0 displays the most dynamic and visually distinct reversible color transitions, cycling through yellow, brown, white, and bronze states (Figure. 2a), proving to be an ideal model system for elucidating real-time structural optical dynamics.

The *in-situ* GIWAXS patterns (Figure 2c-f) and their intensity (Figure 2g and h), which are precisely matched to each optical state, directly visualize the structural origins of this multicolor chromism. Upon hydration, the diffraction peak corresponding to the layered 2D-related motif (004) is rapidly suppressed within 100 seconds, only to re-emerge immediately

upon nitrogen (N_2) drying. Conversely, the primary diffraction feature of the 1D-related framework ($q \approx 0.81$ Å^{-1}) persists without collapsing throughout the humidity cycles, accompanied only by azimuthal broadening that implies lattice reorientation. Most notably, the PbI_2 peak ($q \approx 0.9$ Å^{-1})[36,37], clear evidence of chemical degradation[38], was completely absent during the entire cycling process. This absence, coupled with rigorous control experiments using pure PbI_2 films (Figure S6), strongly corroborates that the observed structural transformations rather than moisture-induced chemical degradation (Figure 2b).

To most compellingly demonstrate that this phenomenon is an intrinsic structure–property coupling rather than material decomposition, we perfectly synchronized the structural data from *in-situ* GIWAXS and the optical data from UV-vis spectroscopy on a single time axis (Figure. 2h, j). When hydration causes a sharp attenuation in the integrated diffraction intensity of the 2D structure, the optical absorption edge near 500 nm collapses simultaneously, and the spectrum is reorganized to be dominated by the 1D-related short-wavelength absorption band around 380 nm. Conversely, during drying, the recovery of the 2D diffraction peak and the gradual restoration of the long-wavelength absorption band follow precisely matching trajectories.

Ultimately, this perfect real-time synchronization between structural dynamics and optical transitions unequivocally confirms that the observed macroscopic chromism is not a consequence of chemical degradation. Rather, it provides definitive evidence of a rapid, non-destructive, and reversible lattice reorganization between 1D- and 2D-related motifs. This dynamic process is mediated by environmental humidity and enabled by the inherent structural flexibility afforded by the EA cations.

While our *in-situ* measurements firmly establish the reversibility and reproducibility of these transformations, the precise crystallographic nature of the intermediate bronze state (characterized by the ~400 nm optical feature) and the exact molecular-level role of water remain unresolved. In addition, the subtle splitting observed in the (004)* peak, presumably originating from hydration-induced strain, warrants further investigation to fully elucidate its underlying crystallographic origin. Future investigations addressing these open questions will be critical for determining the universality of this dynamic behavior across the broader compositional space of EA-based perovskites.

2.3. Uncovering the hidden variable: Stoichiometry-gated threshold

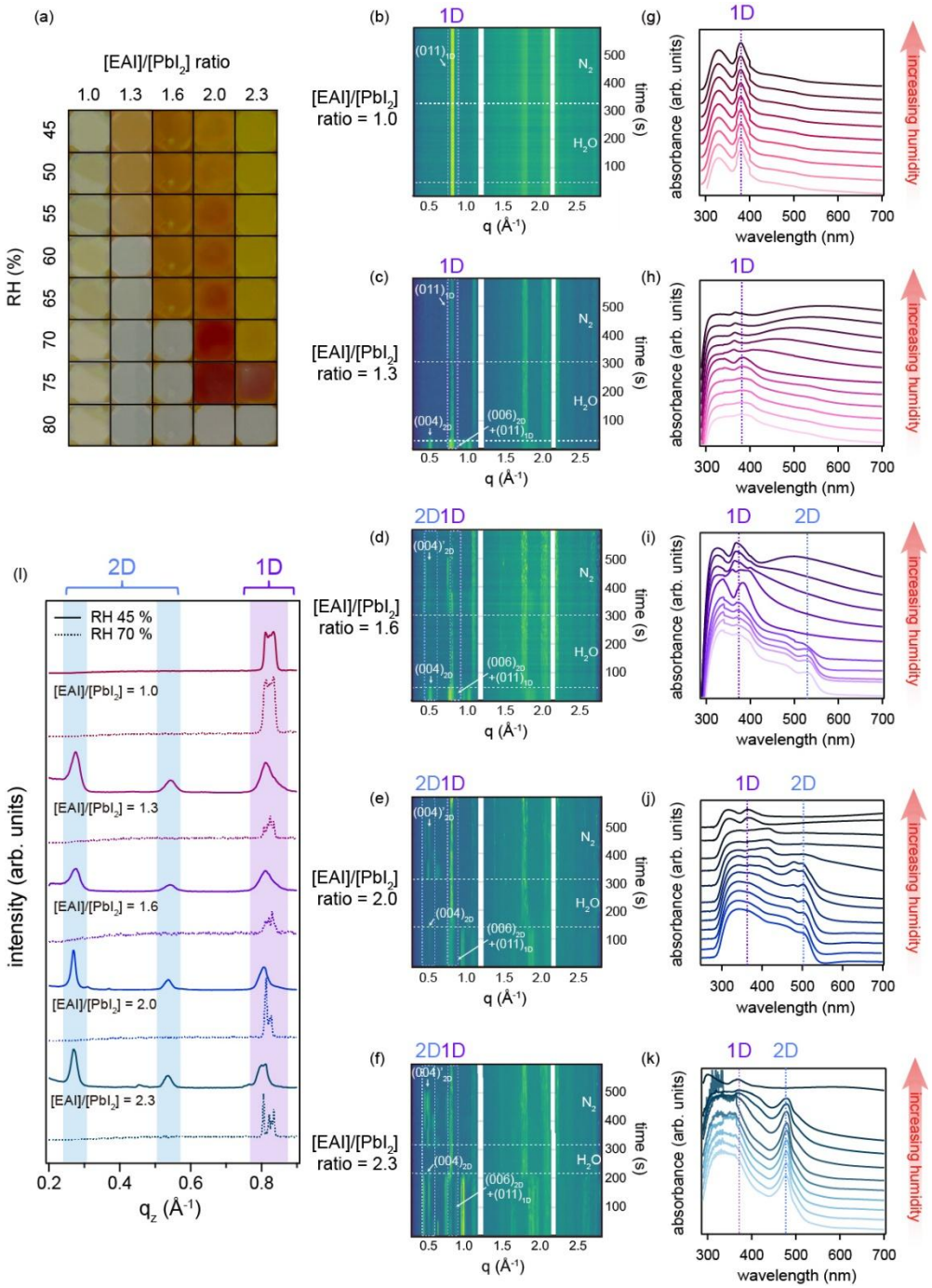


Figure 3 | Stoichiometry-gated threshold for reversible humidity-driven phase dynamics in EA-based perovskites. (a) Optical color map of EA-based perovskite thin films synthesized with systematically varied [EAI]/[PbI_2] ratios and relative humidity (RH). (b–f) *In-situ* GIWAXS intensity heatmaps and (g-k) *In-situ* UV–visible absorption spectra collected during repeated humidity modulation (1st cycle from 45% to 70%) for films with [EAI]/[PbI_2] ratios ranging from 1.0 to 2.3. The other cycle spectra provided in Figure S10. **(l)** Out-of-plane 1D GIWAXS diffraction profiles acquired at RH 45% (solid lines) and 70% (dashed lines).

In the preceding section, we confirmed the complete structural and optical reversibility of a specific composition ([EAI]/[PbI_2] = 2.0). However, determining whether this dynamic phenomenon is a universal characteristic of EA-based perovskites or merely restricted to specific conditions is essential for understanding the conflicting reports in existing literature. To clarify this, we systematically varied the [EAI]/[PbI_2] ratio from 1.0 to 2.3 and continuously tracked the structural and optical behaviors under cyclic humidity (RH 45% ↔ 70%).

As clearly depicted in the optical color map (Figure 3a), the humidity responsiveness of the films exhibits a stark composition-dependent transition. The structural origins of this composition-dependent reversibility are starkly differentiated in the *in-situ* GIWAXS intensity heatmaps acquired during repeated humidity modulation (Figure 3b–f). Compositions below the threshold ([EAI]/[PbI_2] ratio of 1.0 and 1.3) maintain static diffraction features or suffer a non-recovering structural collapse upon hydration. Conversely, compositions of [EAI]/[PbI_2] of 1.6 and above undergo pronounced, perfectly synchronized, and reversible structural reconfigurations between 1D- and 2D-related motifs. This unequivocally demonstrates the existence of a stoichiometry-gated threshold near [EAI]/[PbI_2] ≈ 1.6, which activates the reversible humidity-driven phase dynamics.

The physical significance of this threshold is further corroborated by *in-situ* UV-vis absorption spectra (Fig. 3g–k). The initial spectra measured under dry conditions (RH 45%) reveal that, directly correlating with the onset of structural reversibility ([EAI]/[PbI_2] ≥ 1.6), a distinct absorption edge emerges near 500 nm, accompanied by systematic spectral broadening. This indicates that a sufficient EA cation is required to form a mixed-dimensional landscape capable of accommodating dynamic reconfigurations, thereby serving as a structural prerequisite for reversibility. Interestingly, for compositions exhibiting reversible behavior, the out-of-plane 1D GIWAXS diffraction profiles acquired under high humidity (RH 70%, Figure 3l) converge toward the characteristic structural fingerprint of pure 1D structure independent of the initial precursor ratio. This implies that upon moisture exposure, the systems reach a common reversible structural endpoint of a pure 1D structure, regardless of the amount of EA cation.

Consequently, the stoichiometry-gated threshold identified in this study perfectly elucidates the severe discrepancies regarding the structural properties of EA-based perovskites reported in the literature[27-30]. Previous investigations failed to recognize the interplay between uncontrolled environmental humidity, which varies across laboratories and seasons, and the precursor ratio (the threshold at 1.6), which acts as a structural switch governing humidity

responsiveness[27-30]. Therefore, when static samples prepared at stoichiometric ratios (e.g., [EAI]/[PbI_2] ratio of 1.0) and dynamic samples containing EA cation above the threshold were exposed to varying ambient humidities, they were reported as exhibiting completely different structural stabilities and degradation behaviors, despite being the identical fundamental material. Our discovery that the precursor ratio functions as a gate for this hidden environmental variable provides the definitive key to concluding the long-standing academic controversy surrounding perovskite phase behavior.

2.4. Mechanistic framework of moisture-driven reconfigurability

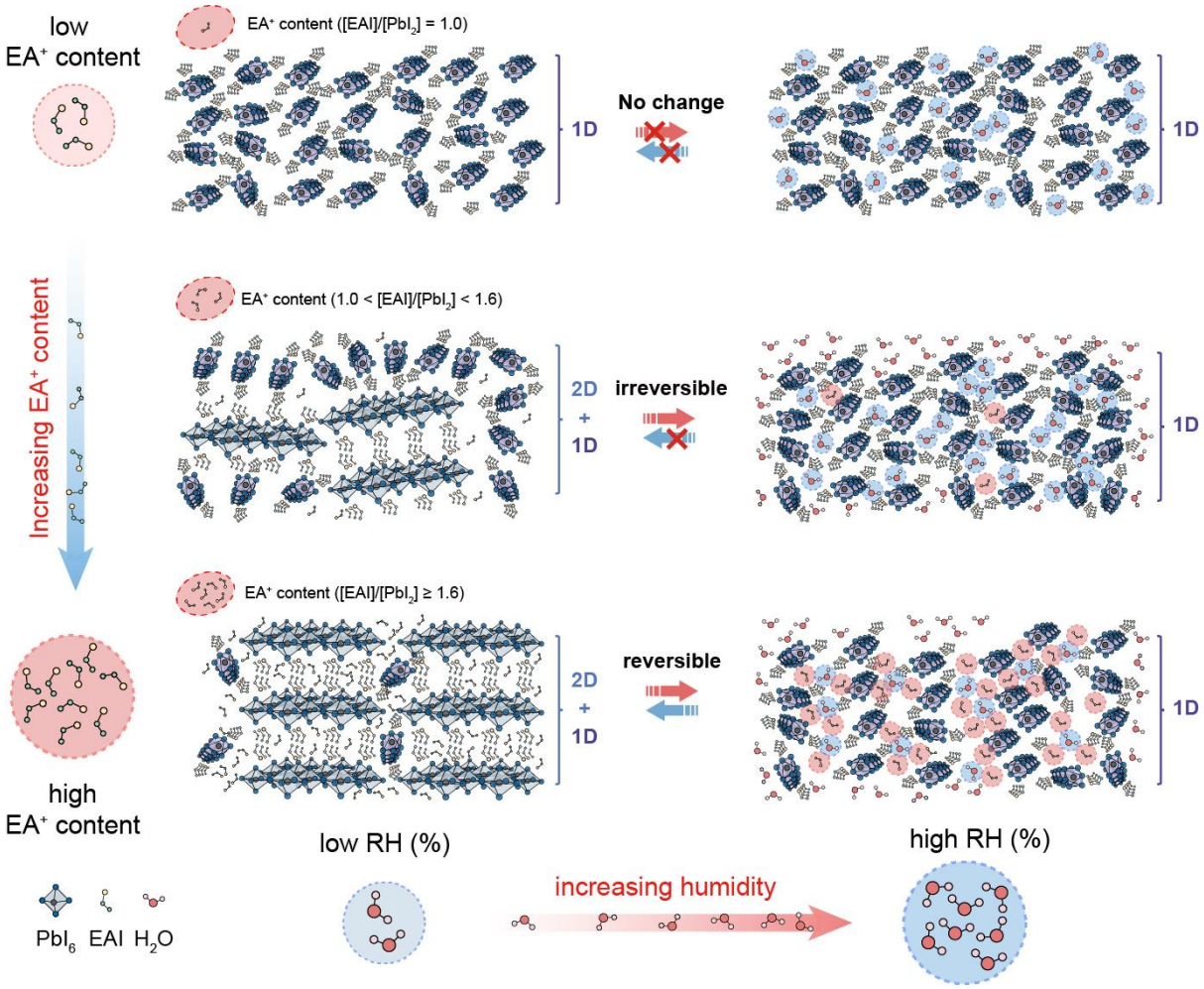


Figure 4 | Proposed mechanistic framework for composition- and humidity-dependent lattice reconfiguration in EA-based perovskites. Schematic illustration summarizing the composition- and humidity-dependent lattice response of EA-based perovskites. (Top) At [EAI]/[PbI_2] ratio of 1.0, the lattice adopts a predominantly 1D-related framework that remains largely insensitive to humidity. (Middle) Below the reversibility threshold (1.0 < [EAI]/[PbI_2] < 1.6), mixed 1D/2D-related structural motifs emerge, giving rise to partial and non-recovering lattice rearrangements under humidity. (Bottom) Above the reversibility threshold ([EAI]/[PbI_2] ≥ 1.6), enhanced structural flexibility enables reversible lattice reconfiguration between competing 1D- and 2D-related motifs upon hydration and dehydration, leading to repeatable and non-destructive chromic responses.

Building upon the perfect structural–optical synchronization established via *in-situ* GIWAXS and UV–vis spectroscopy, we propose a physical mechanistic model (Figure 4) to elucidate the moisture-driven reversible lattice rearrangement. The crux of this framework is that the

Ethylammonium (EA^+) cations, finely tuned by precursor stoichiometry, function not merely as additives, but as a structural buffer that accommodates the ingress and egress of water molecules while preventing the collapse of the inorganic lattice.

In the [EAI]/[PbI_2] ratio of 1.0, the perovskite framework is strictly confined to a rigid 1D network. These inorganic PbI_6 chains are completely surrounded by organic cations, creating a sterically hindered environment that lacks sufficient free volume[39]. This structural rigidity renders the lattice humidity-inert, effectively preserving its pristine 1D framework against water intercalation even under moisture exposure. Below the threshold ([EAI]/[PbI_2] < 1.6), the perovskite framework enters a state where 1D and 2D structures coexist. However, the limited amount of organic spacers is insufficient to provide a structural buffer. Upon moisture exposure, the penetrating water molecules exert localized strain that induces the 2D motifs to undergo an irreversible transformation into 1D chains. Consequently, the framework fails to revert to its pristine 1D and 2D mixed state even after water desorbs, remaining in a fixed 1D-dominant configuration.

Conversely, above reversibility threshold ([EAI]/[PbI_2] ≥ 1.6), the lattice dynamics are fundamentally inverted. The abundant organic cations intercalate between the inorganic octahedral chains, forming a mixed-dimensional landscape where 1D and 2D motifs coexist, thereby maximizing the softness of the lattice.[40] Upon exposure to humidity, these expanded organic spacer layers serve as a dynamic buffer zone that accommodates the penetrating water molecules. Rather than breaking the bonds of the inorganic framework to cause chemical decomposition (i.e., PbI_2 formation), the intercalated water acts as a transient external stimulus. Assisted by the organic buffer layer, it guides the inorganic chains to smoothly slide and reorganize from a 1D- to a 2D-related layered arrangement. Subsequently, as water molecules gently desorb during the nitrogen (N_2) purging and drying process, the lattice reverts to its pristine 1D-dominant configuration, thereby completing a non-destructive dynamic lattice reorganization.

The remarkable multicolor chromism observed in this compositional regime is not the physical manifestation of a single static phase. Rather, it is the macroscopic optical manifestation of a continuously shifting "dynamic equilibrium" between competing 1D and 2D structural motifs in response to the adsorption and desorption of water, which precisely modulates the local octahedral arrangements. Taken together, this proposed mechanistic framework establishes precursor stoichiometry as an essential design parameter governing the environmental

responsiveness of EA-based perovskites. Although the precise crystallographic determination of the hydrated intermediate (bronze state) and the microscopic hydrogen-bonding interactions between water molecules and EA cations remain subjects for future high-resolution spectroscopic and theoretical investigations (e.g., density functional theory calculations), the structural buffer mechanism derived herein provides a robust theoretical foundation for designing dynamically reconfigurable perovskite materials that actively respond to environmental stimuli.

2.5 Demonstration of humidity-responsive smart devices

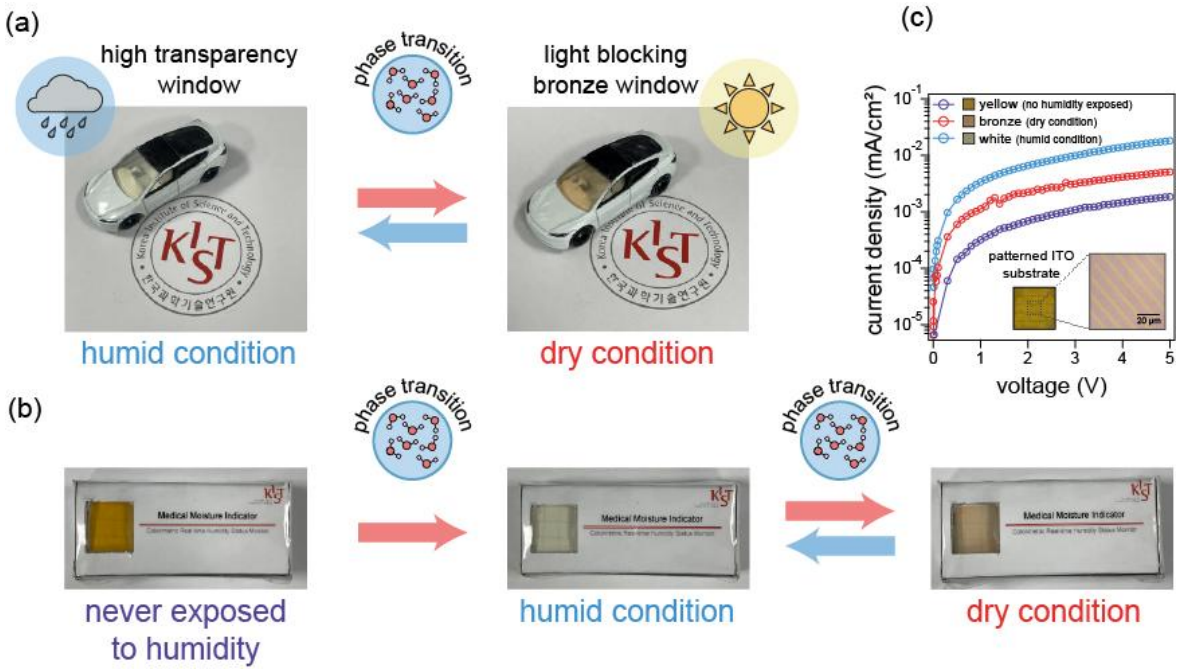


Figure 5 | Demonstration of humidity-responsive smart devices: autonomous smart windows and dual-functional medical moisture indicators. (a) Prototype of a moisture-responsive smart car window adapting to external environmental changes. Under dry, sunny conditions (right), the window adopts a light-absorbing bronze state to maintain optimal interior illuminance. On highly humid days, such as rainy or cloudy weather (left), the window autonomously transitions to a highly transparent state, maximizing external light transmission into the vehicle interior. (b) Application of the film as a medical moisture exposure indicator. The pristine yellow state (left) guarantees that the package has never been exposed to external humidity. Upon exposure to ambient humidity (>60% RH) for over 100 s (middle), the film undergoes an irreversible transition, permanently losing its initial yellow color. Subsequently, it functions as a real-time humidity sensor, dynamically switching between transparent (at high humidity, ~70% RH, right) and bronze states to visually indicate current environmental conditions. **(c)** Current–voltage (I–V) characteristics of the medical indicator corresponding to different moisture exposure states. The insets in (c) show a photo of the device and a magnified view of the active region. The distinct variations in electrical current provide a quantifiable electronic readout of the moisture exposure level, complementing the macroscopic optical changes.

The stoichiometry-driven reversible lattice rearrangement mechanism, elucidated above, suggests that EA-based perovskites are promising candidates for zero-power, environment-responsive smart devices. To demonstrate the practical impact of this material, we leveraged its unique hydrochromism to successfully fabricate an autonomous smart window and a dual-

functional medical moisture exposure indicator.

Figure 5a illustrates the operation of a smart car window prototype that autonomously adapts to external weather conditions. Under clear and dry conditions (intense sunlight), the window maintains a light-absorbing brown state, acting as a sunshade to prevent internal glare and maintain optimal interior illuminance. Conversely, in highly humid environments, such as rainy or cloudy days, the window senses the ambient humidity and autonomously transitions to a highly transparent state. This serves as a successful demonstration of active optical modulation, maximizing the influx of external light in response to weather changes solely through the intrinsic phase-transition properties of the material, circumventing the need for complex external power supplies or electronic control systems.

Furthermore, we designed a medical moisture exposure indicator with temper-evident security features by exploiting the unique transition trajectory of this material: the initial irreversibility when shifting from the pristine yellow state to the multicolor hydrochromic phase (white ↔ bronze), followed by its subsequent dynamic reversibility (Figure 5b). When attached inside the packaging of vaccines or moisture-sensitive pharmaceuticals, the intact yellow state of the indicator visually guarantees that the product has never been exposed to external humidity since its dispatch.

However, if the seal is compromised and the indicator is exposed to an ambient humidity of over 60% for more than 100 s, the film undergoes an irreversible lattice transition, permanently losing its pristine yellow color. This "irreversible history logging" function provides an absolute fail-safe criterion for determining product degradation. Once compromised and the yellow color is lost, the indicator switches into a real-time humidity sensor mode, continuously visualizing the current internal humidity by dynamically oscillating between a bronze state (dry) and a highly transparent state (~70% RH, high humidity).

More importantly, these macroscopic optical color changes are accompanied by distinct modulations in electrical properties. The current–voltage (*I–V*) characteristic curves of the indicator under different moisture exposure states (Figure 5c) reveal that the device's electrical current values are clearly distinguishable based on its humidity exposure history. Notably, the sensor demonstrates high sensitivity with nearly an order of magnitude difference in electrical current between the bronze (dry) and transparent (humid) states at a bias of 5 V. This signifies that, moving beyond qualitative visual color changes, the sensor can be integrated into smart

packaging systems to translate the moisture exposure level into a quantifiable electronic readout.

In conclusion, these proof-of-concept demonstrations establish that the properties of boundary-region perovskites, previously considered structurally ambiguous and notoriously difficult to handle, can be successfully translated into innovative active environmental sensing technologies. By turning instability into functionality through precise stoichiometric control, the approach presented in this study offers a new design paradigm for next-generation smart optoelectronic devices and environmental monitoring systems.

3. Conclusion

In conclusion, this study fundamentally resolves the long-standing structural ambiguity surrounding Ethylammonium (EA)-based perovskites by identifying environmental humidity as a hidden variable governed by precursor stoichiometry. Contrary to conventional understanding, we demonstrate that at specific stoichiometric thresholds ([EAI]/[PbI_2] ≥ 1.6), moisture does not induce chemical degradation into PbI_2 but instead triggers a rapid, non-destructive, and fully reversible lattice reconfiguration between 1D- and 2D-related motifs. This phenomenon is a direct consequence of the intrinsic dynamic lattice rearrangement mechanism, where EA cations act as structural buffers to establish a flexible, mixed-dimensional landscape.

Leveraging the perfect reversibility of this internal lattice dynamics and its precise structural–optical synchronization, we successfully demonstrated practical, zero-power, humidity-responsive smart devices. The implementation of an autonomous smart window prototype and a dual-functional medical indicator, capable of both irreversible history logging and real-time quantitative monitoring, underscores the exceptional practical utility of this material.

The impact of these findings extends beyond the specific case of EA-based systems. This work offers a transformative perspective on perovskite materials residing at the extreme boundaries of the Goldschmidt tolerance factor, which have traditionally been considered notoriously difficult to stabilize. By turning instability into innovative functionality, we have established a universal methodology to harness inherent structural flexibility as a robust platform for active environmental sensing and the design of next-generation smart optoelectronic devices.

4. Method and Experiment section

4.1. Materials

Ethylammonium iodide (EAI) was purchased from Greatcell Solar. Lead(II) iodide (PbI_2) was obtained from Alfa Aesar. Dimethylformamide (DMF), dimethyl sulfoxide (DMSO), and chlorobenzene (CB) were purchased from Sigma-Aldrich.

4.2. Sample preparation

All perovskite thin film was synthesized by mixing the organic iodide compounds and PbI_2 in the ratios specified in the main text. The precursor solution was prepared in a mixed solvent of dimethylformamide (DMF) and dimethyl sulfoxide (DMSO) with a volume ratio of 5:1. The precursor solutions were deposited onto indium tin oxide (ITO)-coated glass substrates via spin coating. The ITO substrates were cleaned using a standard procedure involving detergent, deionized (DI) water, acetone and ethanol, followed by UV-ozone treatment at 100 °C for 15 min. Spin coating was performed in two steps: 1,000 rpm for 10 s and 5,000 rpm for 60 s. At 40 s before the end of the spin-coating process, 200 μL of chlorobenzene was rapidly dropped onto the surface as an antisolvent. Immediately after spin coating, the samples were transferred to a hot plate and annealed at 85 °C for 20 min.

4.3. GIWAXS characterization

Grazing incidence wide angle X-ray scattering (GIWAXS) measurements were carried out at the 3C SAXS beamline of the Pohang Accelerator Laboratory (PAL), Pohang, Republic of Korea, using an incident photon energy of 11.3 keV ($\lambda = 1.097$ Å). The X-ray beam was focused to approximately 350 × 100 μm² at the sample position, and the instrumental contribution to the scattering vector resolution was estimated to be $\Delta q \approx 0.01 \times 0.0035$ Å^{-1}, which is negligible compared with the intrinsic broadening of the samples. The samples were positioned 213 mm from the detector, and the scattered signals were recorded using an Eiger X4M detector (Dectris) with a pixel size of 75 × 75 μm². To enable in situ humidity control during GIWAXS measurements, a custom-modified environmental chamber compatible with the 3C beamline geometry was used (Figure S3). During the measurements, the relative humidity (RH) inside the sample chamber was alternated between 45% and 70% using a humidifier controlled by a

humidity controller connected to an internal humidity sensor. The chamber humidity was reduced by flowing nitrogen gas, and once 45% RH was reached, the gas flow was gradually reduced to stabilize the humidity at 70% RH (Figure S5). To investigate the impact of high-intensity synchrotron radiation on the structure of EA-based perovskites, we performed a beam damage assessment under continuous exposure; no significant beam damage was observed under our experimental conditions. (Figure S7)

4.4. Optical characterization

UV-visible absorption spectra were recorded using a V-730 double-beam UV-visible spectrophotometer (JASCO, Japan). All measurements were conducted in transmission mode, with a bare ITO-coated glass substrate used as the reference for baseline correction. In-situ UV-visible measurements were performed under nominally identical relative humidity conditions as those used for GIWAXS measurements, using a separately modified optical chamber (Figure S4).

Data Availability Statement

The data that support the findings of this study are available from the corresponding author upon reasonable request.

Acknowledgements

The authors thank the Pohang Accelerator Laboratory (PAL) and Helmholtz-Zentrum Berlin (HZB) for allocating synchrotron radiation beam time at PAL 3C (Korea) and Bessy II ENERGIZE endstation (Germany).

Funding

This work was supported by the National Research Foundation of Korea [RS-2025-25442614 (50%), RS-2024-00449682, and RS-2025-00506764], and Samsung Electronics.

Conflict of interest

The authors declare no competing financial interests.

Supporting Information

Supporting Information is available free of charge on the online.

Author contribution

S.K., K.K., Y.Y., and D.S. conceived the idea and designed the study. E.Y. and S.Y.P. provided technical support for the GIWAXS and XPS measurements. Y.Y.K. contributed to the interpretation of the GIWAXS data. Y.Y.K., K.H.L. and S. Park supervised the project and editing of the manuscript. All authors discussed the results and commented on the manuscript.

Keywords

Dynamic lattice rearrangement, Multicolor hydrochromism, Goldschmidt boundary-region perovskites, Ethylammonium perovskites, humidity responsive devices

References

[1] Chen, Y. *et al.* 2D Ruddlesden–Popper Perovskites for Optoelectronics. *Advanced Materials* **30**, 1703487 (2018).

[2] Mao, L., Stoumpos, C. C. & Kanatzidis, M. G. Two-Dimensional Hybrid Halide Perovskites: Principles and Promises. *Journal of the American Chemical Society* **141**, 1171–1190 (2019).

[3] Yoo, J. J. *et al.* Efficient perovskite solar cells via improved carrier management. *Nature* **590**, 587–593 (2021).

[4] Min, H. *et al.* Perovskite solar cells with atomically coherent interlayers on SnO2 electrodes. *Nature* **598**, 444–450 (2021).

[5] Grancini, G. & Nazeeruddin, M. K. Dimensional tailoring of hybrid perovskites for photovoltaics. *Nature Reviews Materials* **4**, 4–22 (2018).

[6] Li, W. *et al.* Chemically diverse and multifunctional hybrid organic–inorganic perovskites. *Nature Reviews Materials* **2**, 16099 (2017).

[7] Chu, Z. *et al.* Large cation Ethylammonium incorporated perovskite for efficient and spectra stable blue light-emitting diodes. *Nature Communications* **11** (2020).

[8] Jung, M.-H. Exploration of two-dimensional perovskites incorporating methylammonium for high performance solar cells. *CrystEngComm* **23**, 1181–1200 (2021).

[9] Nishi, K., Oku, T., Kishimoto, T., Ueoka, N. & Suzuki, A. Photovoltaic Characteristics of $CH_3NH_3PbI_3$ Perovskite Solar Cells Added with Ethylammonium Bromide and Formamidinium Iodide. *Coatings* **10**, 410 (2020).

[10] Azmi, R., Utomo, D. S., Liu, Y., Zhumagali, S. & De Wolf, S. Dimensionality engineering of perovskites for stable heterojunction-based photovoltaics. *Nature Reviews Materials* **11**, 136–155 (2025).

[11] Goldschmidt, V. M. Die Gesetze der Krystallochemie. *Die Naturwissenschaften* **14**, 477–485 (1926).

[12] Kieslich, G., Sun, S. & Cheetham, A. K. Solid-state principles applied to organic–inorganic perovskites: new tricks for an old dog. *Chem. Sci.* **5**, 4712–4715 (2014).

[13] Bartel, C. J. *et al.* New tolerance factor to predict the stability of perovskite oxides and halides. *Science Advances* **5**, eaav0693 (2019).

[14] Liu, D. *et al.* Structural Properties and Stability of Inorganic $CsPbI_3$ Perovskites. *Small*

Structures **2**, 2000089 (2021).

[15] Li, Y. *et al.* Formamidinium-Based Lead Halide Perovskites: Structure, Properties, and Fabrication Methodologies. *Small Methods* **2**, 1700387 (2018).

[16] Lin, J. *et al.* Thermochromic halide perovskite solar cells. *Nature Materials* **17**, 261–267 (2018).

[17] Lassoued, M. S. *et al.* Reversible thermochromism, temperature-dependent conductivity and high stability for a laminated bismuth(iii)–silver(i) hybrid double perovskite. *Journal of Materials Chemistry C* **10**, 12574–12581 (2022).

[18] Du, Y. *et al.* Perovskite-Coated Thermochromic Transparent Wood: A Novel Material for Smart Windows in Energy-Efficient and Sustainable Buildings. *ACS Applied Materials & Interfaces* **15**, 49665–49677 (2023).

[19] Jaffe, A. *et al.* High-Pressure Single-Crystal Structures of 3D Lead-Halide Hybrid Perovskites and Pressure Effects on their Electronic and Optical Properties. *ACS Central Science* **2**, 201–209 (2016).

[20] Wang, L., Wang, K. & Zou, B. Pressure-Induced Structural and Optical Properties of Organometal Halide Perovskite-Based Formamidinium Lead Bromide. *The Journal of Physical Chemistry Letters* **7**, 2556–2562 (2016).

[21] Zhang, C. *et al.* Conversion of invisible metal-organic frameworks to luminescent perovskite nanocrystals for confidential information encryption and decryption. *Nature Communications* **8** (2017).

[22] Kanwat, A. *et al.* Reversible Photochromism in ⟨110⟩ Oriented Layered Halide Perovskite. *ACS Nano* **16**, 2942–2952 (2022).

[23] Minh, D. N. *et al.* Low-Dimensional Single-Cation Formamidinium Lead Halide Perovskites ($FA_{m+2}Pb_mBr_{3m+2}$): From Synthesis to Rewritable Phase-Change Memory Film. *Advanced Functional Materials* **31**, 2011093 (2021).

[24] Gu, H. *et al.* Phase-pure two-dimensional layered perovskite thin films. *Nature Reviews Materials* **8**, 533–551 (2023).

[25] Allard, C. 3D to 2D perovskite conversion. *Nature Reviews Materials* **8**, 780–780 (2023).

[26] Travis, W., Glover, E. N. K., Bronstein, H., Scanlon, D. O. & Palgrave, R. G. On the application of the tolerance factor to inorganic and hybrid halide perovskites: a revised system. *Chemical Science* **7**, 4548–4556 (2016).

[27] Muralidhar, J. R. *et al.* Chemical Storage of Ammonia through Dynamic Structural

Transformation of a Hybrid Perovskite Compound. *Journal of the American Chemical Society* **145**, 16973–16977 (2023).

[28] Guvenc, C. M. *et al.* Breaking the Boundaries of the Goldschmidt Tolerance Factor with Ethylammonium Lead Iodide Perovskite Nanocrystals. *ACS Nano* **19**, 1557–1565 (2025).

[29] Surel, J. L., Cutlip, E. V., Mandeville, J. R. & Christians, J. A. Switchable Color Semiconductors: Methylamine Intercalation, Deintercalation, and Retention in Two-Dimensional Halide Perovskites. *ACS Applied Energy Materials* **5**, 12029–12038 (2022).

[30] Zhou, J. *et al.* Efficient ambient-air-stable HTM-free carbon-based perovskite solar cells with hybrid 2D–3D lead halide photoabsorbers. *Journal of Materials Chemistry A* **6**, 22626–22635 (2018).

[31] Zhang, F. *et al.* Moisture-Induced Reversible Phase Conversion of Cesium Copper Iodine Nanocrystals Enables Advanced Anti-Counterfeiting. *Advanced Functional Materials* **31**, 2105771 (2021).

[32] Rosales, B. A. *et al.* Reversible multicolor chromism in layered formamidinium metal halide perovskites. *Nature Communications* **11** (2020).

[33] Yu, X. *et al.* Hydrochromic $CsPbBr_3$ Nanocrystals for Anti-Counterfeiting. *Angewandte Chemie* **132**, 14635–14640 (2020).

[34] Chen, J. *et al.* Hydrochromic Perovskite System with Reversible Blue-Green Color for Advanced Anti-Counterfeiting. *Small* **19** (2023).

[35] Niu, G. *et al.* Study on the stability of $CH_3NH_3PbI_3$ films and the effect of post-modification by aluminum oxide in all-solid-state hybrid solar cells. *J. Mater. Chem. A* **2**, 705–710 (2014).

[36] Xiong, Z. *et al.* Simultaneous Interfacial Modification and Crystallization Control by Biguanide Hydrochloride for Stable Perovskite Solar Cells with PCE of 24.4%. *Advanced Materials* **34**, 2106118 (2022).

[37] Wang, D. *et al.* Various Mechanisms of Additives in Different Additive Methods on the Crystallinity of Perovskite by Synchrotron Radiation Technology. *Advanced Optical Materials* **12** (2024).

[38] Liang, J. *et al.* Origins and influences of metallic lead in perovskite solar cells. *Joule* **6**, 816–833 (2022).

[39] Kong, T. *et al.* Perovskitoid-Templated Formation of a 1D@3D Perovskite Structure

toward Highly Efficient and Stable Perovskite Solar Cells. *Advanced Energy Materials* **11**, 2101018 (2021).

[40] Min, S., Mukherjee, M., Szabó, G., Kamat, P. V. & Cho, J. Design principles of spacer cations for suppressing phase segregation in 2D halide perovskites. *Chemical Science* **16**, 21950–21961 (2025).

Supplementary Files

This is a list of supplementary files associated with this preprint. Click to download.

- Si.docx